



Article

Micron-Sized Silica-PNIPAM Core-Shell Microgels with Tunable Shell-To-Core Ratio

Keumkyung Kuk¹, Lukas Gregel¹, Vahan Abgarjan¹, Caspar Croonenbrock¹, Sebastian Hänsch² 
and Matthias Karg^{1,*} 

¹ Institut für Physikalische Chemie I: Kolloide und Nanooptik, Heinrich-Heine-Universität Düsseldorf, Universitätsstr. 1, 40225 Düsseldorf, Germany

² Center for Advanced Imaging, Heinrich-Heine-Universität Düsseldorf, Universitätsstraße 1, 40225 Düsseldorf, Germany

* Correspondence: karg@hhu.de; Tel.: +49-211-81-12400

Abstract: Micron-sized hard core-soft shell hybrid microgels are promising model systems for studies of soft matter as they enable in-situ optical investigations and their structures/morphologies can be engineered with a great variety. Yet, protocols that yield micron-sized core-shell microgels with a tailorable shell-to-core size ratio are rarely available. In this work, we report on the one-pot synthesis protocol for micron-sized silica-poly(*N*-isopropylacrylamide) core-shell microgels that has excellent control over the shell-to-core ratio. Small-angle light scattering and microscopy of 2- and 3-dimensional assemblies of the synthesized microgels confirm that the produced microgels are monodisperse and suitable for optical investigation even at high packing fractions.

Keywords: micron-sized core-shell microgels; seeded precipitation polymerization; one-pot synthesis; small-angle light scattering; confocal laser scanning microscopy



Citation: Kuk, K.; Gregel, L.;

Abgarjan, V.; Croonenbrock, C.;

Hänsch, S.; Karg, M. Micron-Sized Silica-PNIPAM Core-Shell Microgels with Tunable Shell-To-Core Ratio.

Gels **2022**, *8*, 516. <https://doi.org/10.3390/gels8080516>

Academic Editor: Ferenc Horkay

Received: 25 June 2022

Accepted: 12 August 2022

Published: 18 August 2022

Publisher's Note: MDPI stays neutral with regard to jurisdictional claims in published maps and institutional affiliations.



Copyright: © 2022 by the authors. Licensee MDPI, Basel, Switzerland. This article is an open access article distributed under the terms and conditions of the Creative Commons Attribution (CC BY) license (<https://creativecommons.org/licenses/by/4.0/>).

1. Introduction

Microgels are colloid-like, deformable and soft objects that have interior structures resembling gel-like characteristics swollen by a solvent in which they are dispersed [1,2]. They belong to a unique class of materials because they exhibit both solid- and liquid-like behavior and have the capability to respond to external stimuli, e.g., temperature [3], pH, and ionic strength [4]. These properties can be tuned by engineering the morphologies [5], composition [6], porosity, and elasticity of the microgels [7]. Due to their tailorable stimuli sensitivity, high colloidal stability, and a broad range of possibilities for various functionalization, the past decades have seen a steadily increasing interest in microgels in applications such as biomedicine, photonic and process technology as well as in fundamental research across disciplines [1]. Among others, inorganic core-polymeric shell microgels, also known as hard core-soft shell microgels, have received significant attention, for example, because of their hybrid properties [8,9], fine-tunable interparticle distance [10] and their potential to be assembled into surprisingly complex microstructures despite their isotropic shape [11,12].

In general, there are two approaches to prepare such core-shell (CS) microgels: “grafting from” and “grafting to” approaches [13,14]. In the “grafting from” approach, the polymer chains grow from the core surface, allowing precise control over the shell thickness [12] with a certain limit. On the other hand, in the “grafting to” approach, pre-formed polymer chains/gels are anchored to/adsorbed onto the core surface. A good example is the free radical precipitation polymerization, which is by far the most widely used synthesis technique that can offer a broader size range as well as various post-modification of polymeric shell morphologies and composition via semi-batch and/or seeded precipitation polymerization methods [15–17]. The post-modification can also be used for the overgrowth of the shell, increasing the overall dimension of the CS microgels, hence the shell-to-core size ratio (δ). CS microgels with dimensions close to the micron regime were

synthesized via multiple-step addition of monomer in the past [18,19]. The micron-sized CS microgels could serve as a very convenient model system because their larger sizes, and thus slower diffusion, can enable in-situ optical investigations using, e.g., optical tweezers, simple light microscopy as well as small-angle light scattering (SALS), which are extensively customizable and cost/time efficient in-house methods. However, one-step synthesis for micron-sized CS microgels with tailorable δ has not been reported yet.

In this study, we present a facile and robust one-pot synthesis protocol to prepare micron-sized, monodisperse CS microgels with controllable δ via a surfactant-free seeded precipitation polymerization. We chose silica as the core material because it is generally biocompatible and can be synthesized with great control over size with low polydispersities, not to mention its facile control over its pore sizes and surface properties via simple silanization chemistry [20,21]. We chose poly(*N*-isopropylacrylamide) (PNIPAM) as the shell material not only because it is one of the most commonly used and well-studied polymers but also because of its thermoresponsive nature around ambient temperature, which could give rise to numerous applications. We have covered core sizes ranging from 245 to 455 nm in diameter with overall hydrodynamic diameter (D_h) of the CS microgels up to approximately 1.2 μm . The swelling capacity of the different samples was studied by temperature-dependent dynamic light scattering (DLS). All prepared colloids show thermoresponsive properties in water due to the lower critical solution temperature (LCST) behavior of PNIPAM. As a proof of concept, the synthesized microgels are assembled into 2D and 3D microstructures. These superstructures were successfully studied by SALS, light microscopy as well as confocal microscopy.

2. Results and Discussion

2.1. Synthesis and Characterization

We used the seeded precipitation polymerization to synthesize CS microgels with differently sized silica cores and thermoresponsive PNIPAM shells of different thicknesses. For such synthesis, silica cores are commonly surface-functionalized with methacrylates to establish covalent bonds to the PNIPAM shell. Especially in the high total solids content (TSC, here defined as the mass of all the suspended and dissolved solids in the sample divided by the total volume of continuous phase—water) regime, this hydrophobic surface modification can hamper colloidal stability during the synthesis, which can lead to mixed species with double/triple cores, high polydispersity or macroscopic aggregates. Previously, Karg et al. reported significantly lower encapsulation rates with increasing size of the silica cores [22]. In that study, silica cores with sizes ranging from 68 nm to 170 nm in diameter were used. In more recent studies, silica cores with a size of 351 nm were successfully encapsulated in PNIPAM shells leading to micron-sized CS microgels ($D_h \approx 1 \mu\text{m}$) via seeded precipitation polymerization with multiple-step monomer addition for overgrowing of the shell in the presence of surfactant [19,23]. Others have also reached microgel dimensions on the order of 1 μm via continuous feeding of the monomers in the absence of surfactant [18]. However, precise control over the δ targeting overall dimensions reaching the micrometer regime still seems to be challenging, in particular for one-pot reactions, also known as single batch polymerizations. In this study, we aim to tackle this challenge and propose a simple but robust synthesis route for micron-sized CS microgels that are sufficiently large to be suitable for investigations using light—either in optical microscopy or diffraction. For the preparation of micron-sized CS microgels, we have found that the shell growth is significantly more effective in the lower TSC regime in the absence of surfactant under efficient stirring. Figure 1 shows representative transmission electron microscopy (TEM) images for small (245 nm), medium (388 nm), and large (455 nm) silica cores and the corresponding CS microgels with different shell thicknesses synthesized via surfactant-free precipitation polymerization at low TSC (the proposed synthesis protocol, more details can be found in the Section 4). All CS microgels are labeled using C_xS_y , where x represents the silica core diameter as determined from TEM and y corresponds to the shell-to-core size ratio, δ . δ is defined as D_h measured by dynamic light scattering at 20 °C

(swollen state) divided by the diameter of the silica core measured by TEM, for example, 245 nm core with δ of 2.9 ($C_{245}S_{2.9}$) and 455 nm core with δ of 2.3 ($C_{455}S_{2.3}$). All δ values were calculated with D_h as acquired and without error propagation, see Supplementary information (SI) for more details. The differently sized silica cores in (Figure 1A–C) possess spherical shape and low dispersity in size. In images (Figure 1D–I), the lower contrast area on the edge of the silica cores evidently shows that the PNIPAM encapsulation was successful. In particular, for the microgels with the thickest shells (Figure 1H,I), the shells are clearly visible. Here, each silica core is surrounded by a homogeneous PNIPAM shell. For the microgels with thinner shells, the boundary between the higher electron density—rigid cores, and the low electron density polymeric shell is less noticeable but clearly visible at higher magnification. The TEM images with higher magnifications can be found in SI, Figure S1. We want to note that the samples are imaged in the dried state and under high vacuum conditions in the TEM. Consequently, the shells are imaged in a collapsed state with a much smaller dimension than in bulk dispersion, when the shells are swollen with water.

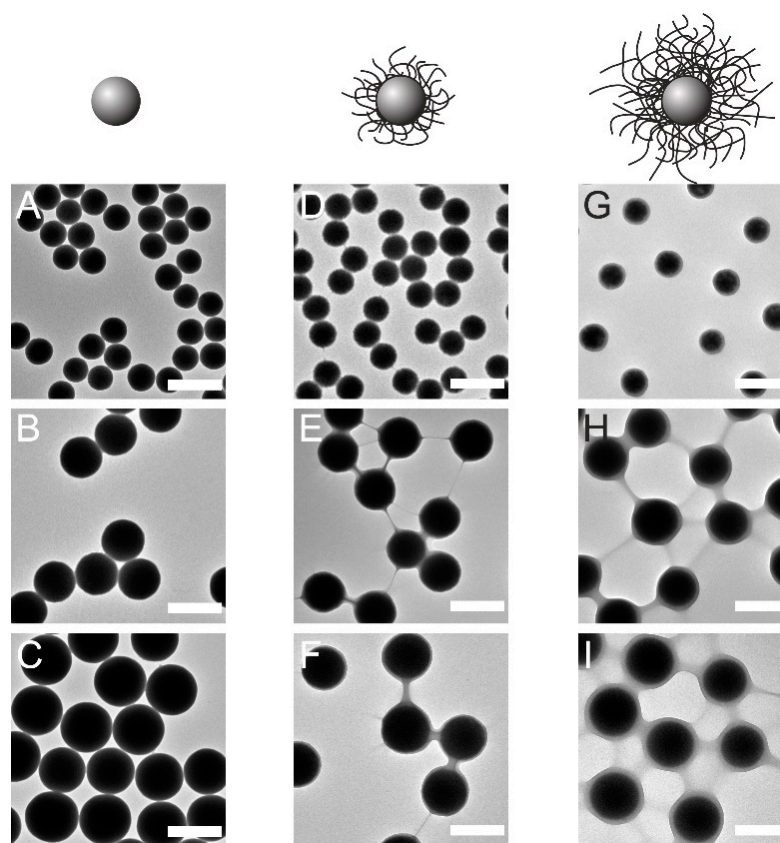


Figure 1. TEM images of CS microgels with variously sized cores: C_{245} (A), C_{388} (B), and C_{455} (C), with thin shells: $C_{245}S_{1.7}$ (D), $C_{388}S_{2.1}$ (E), $C_{455}S_{2.1}$ (F) and with thicker shells: $C_{245}S_{2.9}$ (G), $C_{388}S_{2.6}$ (H), $C_{455}S_{2.3}$ (I). The scale bars correspond to 500 nm.

Figure 2A shows a 3D plot of shell growth on C_{245} in terms of δ as a function of NIPAM concentration per number of core and TSC. The blue spheres represent data for CS microgels synthesized without surfactant in the low TSC regime, using an overhead stirrer (the proposed synthesis protocol), while the green tetrahedrons correspond to results from synthesis with surfactant (sodium dodecyl sulfate-SDS, 2 mM) in the high TSC regime, using a magnetic bar for stirring (following the protocol from [24], labeled as C_xS_y-C for Core-Shell-Conventional). More details on the effects of the individual synthesis parameters such as SDS concentration, stirring method, and temperatures on the overall size of the CS microgels can be found in SI. Figure 2B shows the shell growth in terms of δ as a function of the NIPAM concentration per number of silica cores for the three different core sizes

(see Figure 1) performed via the proposed synthesis protocol at low TSC in the absence of SDS under more efficient stirring. The results show that the synthesis protocol can also be transferred to significantly larger cores. The shell growth of all CS microgels can be described by an exponential growth as a function of monomer concentration per number of cores (fitted with the Gompertz fit, solid lines). This enables us to predict the total microgel sizes for any given feed concentration, at least in the studied range. At the same time, desired values of δ can be specifically targeted. Figure 2C shows the swelling curves of the four selected CS microgels recorded by temperature-dependent DLS: CS microgels with the small core with thin shell $C_{245}S_{1.7}$ (filled blue) and thick shell $C_{245}S_{2.9}$ (empty blue) and the large core with thin shell $C_{455}S_{2.1}$ (filled red) and thick shell $C_{455}S_{2.3}$ (empty red). In all cases, we find the typical volume phase transition (VPT) behavior with a continuous decrease in hydrodynamic diameter with increasing temperature in the vicinity of the volume phase transition temperature (VPTT). Here, we want to note that our larger CS microgels seemed to be under the effect of gravitational settling during the DLS measurements, which could be the reason for their higher polydispersities (or overestimation of polydispersity) compared to the smaller microgels. Although the commonly quoted upper size limit for DLS is around 10 μm , it often is only achievable by increasing the viscosity of the continuous phase or by using capillary DLS [25,26]. In this study, however, we do not further discuss the matter and report the D_h values as recorded and used for the calculation of δ . The calculated de-swelling ratios (α) of the corresponding CS microgels appear to overlap rather well as depicted in Figure 2D. The de-swelling ratios α were calculated as:

$$\alpha = \frac{V_{cs}(T) - V_c}{V_{cs}(10^\circ\text{C}) - V_c} \quad (1)$$

where $V_{cs}(T)$ denotes the volume of the total CS microgel measured by DLS at temperature T , V_c the volume of the non-swelling and non-responsive silica cores measured by TEM.

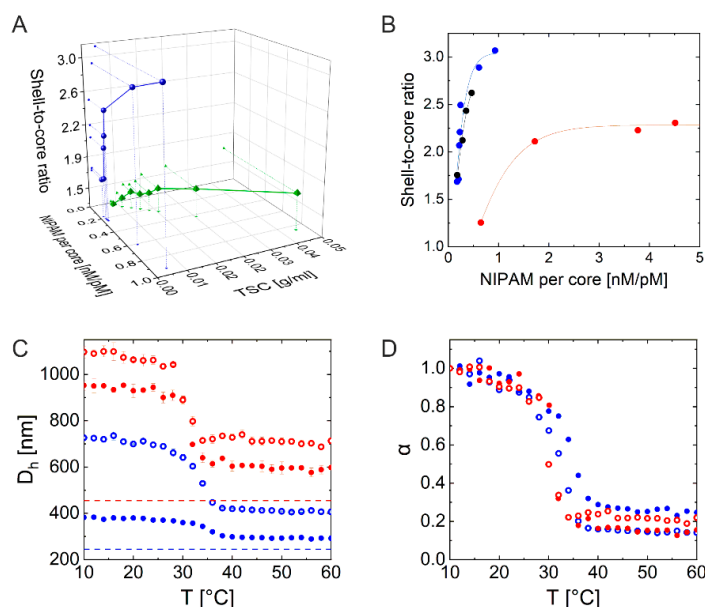


Figure 2. (A) 3D plot of shell growth on C_{245} measured by DLS (depicted as shell-to-core ratio) in dependence of the NIPAM concentration per number of cores in nM/pM and TSC in g/mL. Blue: C_{245} encapsulation via proposed protocol, green: according to [24]. (B) Shell growth on differently sized cores illustrated as the shell-to-core ratio in dependence of the NIPAM feed concentration per number of cores in nM/pM. Blue: C_{245} , black: C_{388} , red: C_{455} . The solid lines correspond to the Gompertz fit of the growth. (C) Swelling curves of $C_{245}S_{1.7}$ (filled blue), $C_{245}S_{2.9}$ (empty blue), $C_{455}S_{2.1}$ (filled red) and $C_{455}S_{2.3}$ (empty red). The dotted lines represent the diameter of the core measured by TEM. (D) Calculated deswelling ratio of corresponding CS microgels from (C).

2.2. Investigation of 2D Assemblies Using Optical Microscopy and SALS

To study 2D assemblies of the CS microgels, we prepared hexagonally ordered monolayers using interface-mediated self-assembly and subsequent transfer to glass substrates. The monolayer assembly is also an effective way to judge their collective behaviors as well as the monodispersity. The samples were transferred to the substrates at surface pressures of approximately 20 mN/m, i.e., at relatively high pressures, where the CS microgels are already in shell-shell contact and squeezed against each other. More information on the sample preparation can be found in the Section 4 and in SI. We prepared monolayers from CS microgels with the smallest ($C_{245}S_{2.9}$) and largest cores ($C_{455}S_{2.3}$) investigated in this study. Figure 3B,E show optical light microscopy images of the samples at 100 \times magnification. For both samples, this magnification is clearly sufficient to resolve single particles. Furthermore, the hexagonal order becomes evident, which is also reflected by the six-fold symmetric fast Fourier transformations (FFTs) shown in (Figure 3A,D). While the microscopic images cover areas on the order of 0.01 mm², we can probe significantly larger areas over 1 mm² when using SALS on the same samples. Figure 3C,F show the recorded diffraction patterns. In both cases, we again see six-fold symmetries, which are in very good agreement with the FFTs computed from the real space images. Thus, optical microscopy and SALS can deliver complementary information despite the different areas probed. We want to highlight that typically microgel and CS microgel assemblies were studied using scattering techniques based on neutrons and/or X-rays (mostly SANS and SAXS) in the past years and/or by rather high-resolution microscopies such as AFM and scanning electron microscopy (SEM). Being able to use light for the structural investigation offers great possibilities for investigation of microstructures and phase transitions in real time being independent of large-scale facilities and expensive setups.

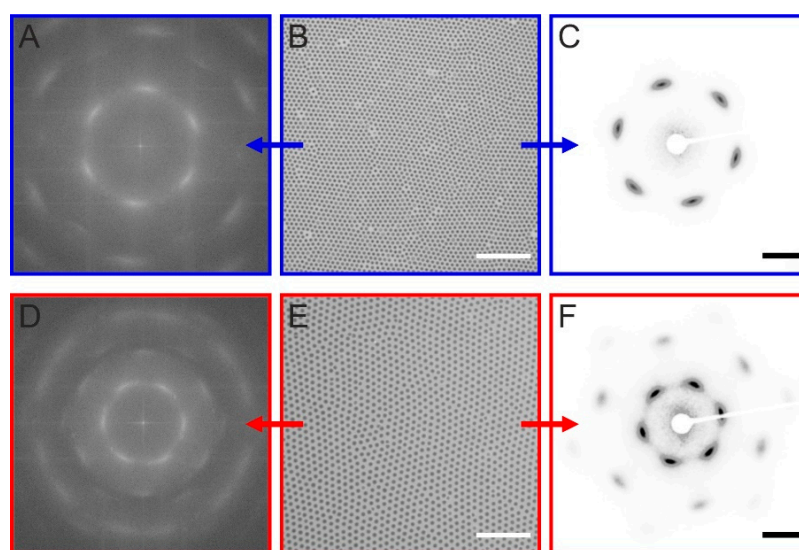


Figure 3. Monolayer analysis by optical light microscopy and SALS. (A) FFT generated from the real space microscopy image of a monolayer prepared from $C_{245}S_{2.9}$ taken at a surface pressure of 20 mN/m (B). (C) Corresponding diffraction pattern recorded by SALS. (D,E) same set of data as in the top row for a monolayer prepared from $C_{455}S_{2.3}$. Scale bars in (B,E) correspond to 10 μ m. Scale bars in (C,F) correspond to 20 mm.

Since the nearest neighbor center-to-center distance, i.e., interparticle distance (D_{c-c}) in 2D assemblies of CS microgels with soft and deformable shells depends on the number of microgels per area, we can cover a broad range of distances with the same batch of microgels simply through adjusting the surface pressure, for example, in a Langmuir trough. Figure 4A shows swelling curves of the two selected CS microgels recorded by temperature-dependent DLS. From these data we can now estimate the possible range of D_{c-c} and area fraction based on two assumptions: (1) The shell deformation at the interface

leads to a microgel diameter that is larger by a factor of 1.76 than the bulk hydrodynamic diameter [24] and the minimum theoretically possible interparticle distance, i.e., D_{c-c} in effective core-core contact, corresponds to the D_h of collapsed CS microgels at 60 °C. (2) The microgels remain perfectly circular and hexagonally arranged throughout the compression, and the defects/empty spaces in the monolayer can simply be reflected by a lower area fraction as expressed in Equations (2) and (3).

$$A_p = \pi \times \left(\frac{D_{c-c}}{2} \right)^2 \quad (2)$$

$$n_p = \frac{A_f \times A_{tot}}{A_p} \quad (3)$$

$$D_{c-c}^2 = \frac{4}{\pi} \times A_f \times \frac{A_{tot}}{n_p} = \frac{4}{\pi} \times A_f \times (n_p/A_{tot})^{-1} \quad (4)$$

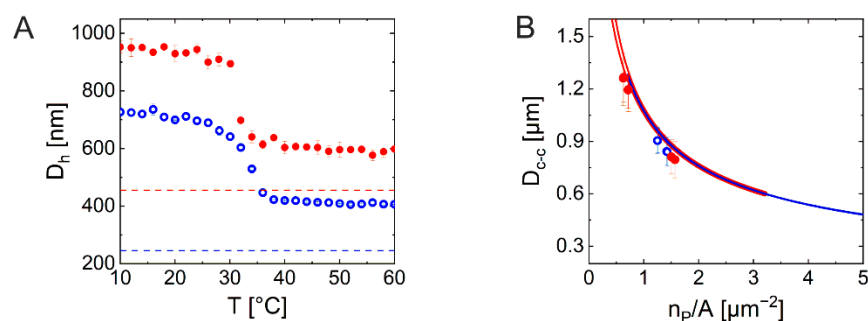


Figure 4. (A) Evolution of the hydrodynamic diameter (D_h) for $C_{245}S_{2.9}$ (blue) and $C_{455}S_{2.3}$ (red) as a function of temperature. The dashed, horizontal lines correspond to the respective core diameters measured by TEM. (B) Calculated interparticle distance (D_{c-c}) against the number of particles per unit area (n_p/A) for 2D compression accounting for an area fraction of 0.91 (solid lines, blue: $C_{245}S_{2.9}$, red: $C_{455}S_{2.3}$). Symbols with error bars: measured data at three different surface pressure (10, 20, and 30 mN/m, blue: $C_{245}S_{2.9}$, red: $C_{455}S_{2.3}$).

Here, A_p denotes the area occupied by one particle, n_p is the number of particles, A_f is the area fraction, and A_{tot} is the total area. It is clear that D_{c-c}^2 scales linear with respect to the area per particle (A_{tot}/n_p), with a slope equal to $4/\pi$ multiplied by A_f . A_f thus can be estimated from the real images. More details on the A_f calculation can be found in SI. Based on these assumptions, we calculated the achievable range of D_{c-c} as a function of the particle number per unit area (n_p/A) in (Figure 4B) (solid lines) at maximum A_f (0.91) for the perfect hexagonal arrangement. The diagram also contains measured values of D_{c-c} (symbols) from monolayers taken from the air/water interface at surface pressures of 10, 20, and 30 mN/m. Note that the measured D_{c-c} lie slightly lower at the same n_p/A values compared to the calculated D_{c-c} , likely due to occasional non-ideal packing or defects of the monolayers. The estimated area fractions are 0.80 for $C_{245}S_{2.9}$ and 0.79 for $C_{455}S_{2.3}$, respectively.

2.3. Investigation of 3D Assemblies Using Confocal Microscopy and SALS

Having shown that our CS microgels are suitable for structural investigations of monolayer samples using light, we now want to turn to 3D assemblies. For this, we chose the sample $C_{340}S_{3.0}$ (silica core dyed with rhodamine B, see SI, Tables S1 and S2 for more details) and prepared variously concentrated dispersions using *N*-methyl-2-pyrrolidone (NMP) as solvent. NMP was chosen to reduce the scattering contrast as NMP has a refractive index (1.47) higher than water (1.33) almost matching the index of PNIPAM (1.50) and silica particles (~ 1.45). This way we could reduce multiple scattering which was necessary for the sample investigation by SALS. The samples were sealed in glass capillary tubes; more details can be found in the Section 4. Figure 5 shows confocal

laser scanning microscopy (CLSM) images obtained from $C_{340}S_{3.0}$ NMP dispersions with two different concentrations. The imaging by CLSM revealed that the sample with the lower concentration had an interparticle distance close to the D_h of its building block with periodical spatial arrangements (Figure 5B), whereas the more concentrated sample showed shorter interparticle distances with amorphous structures (Figure 5E). Both images were taken in the middle of the glass tube and evidently show different spatial arrangements between the two samples. The FFT of image (Figure 5B) has a six-fold symmetry as shown in (Figure 5A), whereas the FFT of image (Figure 5E) shows a diffraction ring as depicted in (Figure 5D), reflecting the amorphous structure. Figure 5C,D show the diffraction patterns recorded from the SALS measurement. The recorded diffraction patterns are in very good agreement with the FFTs of the confocal images. Additionally, we have also acquired z-stacks from one glass wall through the sample to the other glass wall, revealing the spatial arrangement throughout the sample. See SI for the avi files.

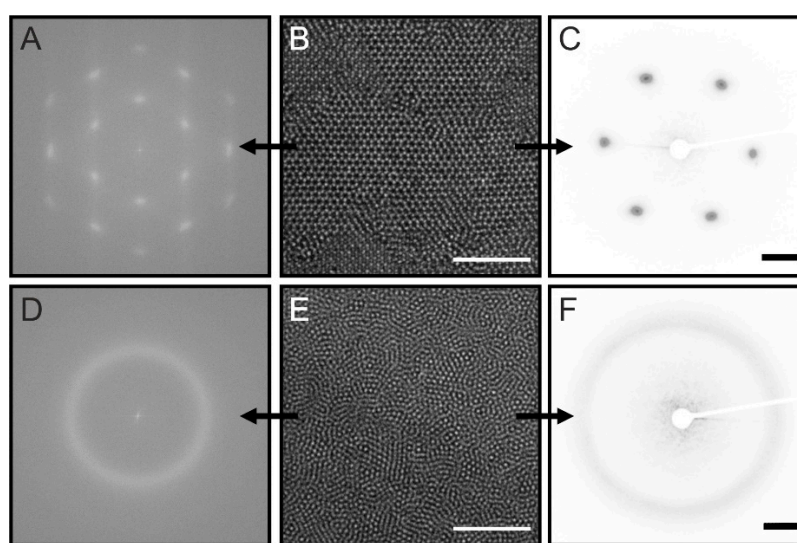


Figure 5. 3D colloidal microstructure analysis by CLSM and SALS (A) FFT calculated from a CLSM image of $C_{340}S_{3.0}$ dispersed in NMP (naturally sedimented from a dilute sample) taken at approximately 58 μm distance from the glass tube wall (B). (C) Corresponding diffraction pattern from SALS performed on the same sample as shown in (B). (D–F) the same set of data as in the top row for $C_{340}S_{3.0}$ dispersed in NMP at a higher concentration taken at approximately 50 μm distance from the glass tube wall (E). The scale bars correspond to 10 μm in (B,E) and to 20 mm in (C,F).

3. Conclusions

In this work, we presented an optimized synthesis protocol that uses the one-pot seeded precipitation polymerization for the preparation of micron-sized core-shell microgels. Silica particles of different sizes were used as rigid cores. The microgel shells were composed of chemically cross-linked poly-*N*-isopropylacrylamide—a thermoresponsive polymer. Due to the single batch nature, our procedure is time- and cost-efficient and offers great control over the shell-to-core ratio. As proof-of-concept experiments to demonstrate the suitability of the microgels for structural investigations using visible wavelength light, we studied substrate-supported monolayers as well as 3D samples in capillaries by confocal laser scanning microscopy and small-angle light scattering. The presented core-shell microgels are not only interesting for photonic applications but also allow convenient microstructural analyses using light rather than X-ray/neutron scattering, enabling cost-/time-efficient in-house investigations of large sample volumes. The presented systems are ideal model colloids to study, for example, interaction potentials of soft microgels with different morphologies under various conditions, their wetting/de-wetting behaviors, melting and crystallization processes as well as jamming transitions.

4. Materials and Methods

4.1. Materials

Ethanol (99.8%, Sigma-Aldrich, Taufkirchen, Germany), ethanol (p.a., Heinrich-Heine-University, chemical store), tetraethyl orthosilicate (TEOS, 98%, Sigma-Aldrich), ammonium hydroxide solution (NH₃ (aq.), 30%, PanReac AppliChem, Darmstadt, Germany), ammonium hydroxide solution (NH₃ (aq.), 25%, VWR, Darmstadt, Germany), hydrogen peroxide solution (H₂O₂, 30 wt %, Fisher Scientific, Schwerte, Germany), *N*-methyl-2-pyrrolidone (NMP, 99.5%, Sigma-Aldrich), rhodamine B isothiocyanate (mixed isomers, Sigma-Aldrich), (3-aminopropyl)trimethoxysilane (97%, Sigma-Aldrich), 3-(trimethoxysilyl)propyl methacrylate (MPS, 98%, Sigma-Aldrich), *N,N'*-methylenebisacrylamide (BIS, 98%, Sigma-Aldrich), sodium dodecyl sulfate (SDS, Ph. Eur., Merck, Darmstadt, Germany), and potassium peroxydisulfate (KPS, 99%, Sigma-Aldrich) were used as received. Water was purified by a Milli-Q system (18.2 MΩ cm) and *N*-isopropylacrylamide (NIPAM, 97%, TCI) by recrystallization from cyclohexane (99.8%, Fisher Scientific).

4.2. Synthesis

4.2.1. Synthesis and Surface Modification of Colloidal Silica Cores

The silica cores were synthesized via the well-known Stöber procedure [27] and surface-modified with MPS. The details of the synthesis protocol have been reported elsewhere. [24] The synthesis conditions and chemicals used are listed in SI, Table S1. Purification of the synthesized silica particles was performed by repeated centrifugation for 2–8 min at 5000–7000 rcf and re-dispersion in ethanol until the supernatant cleared and the smell of ammonia vanished. The concentrated dispersion was stored in ethanol on a 3D shaker. The TSC of the dispersion in g/mL—the amount of solids remaining after storing in the oven at 80 °C for 4 h—was measured three times and averaged. The particle density was assumed to be 2.1 g/mL for the estimation of particle number concentrations [28]. The size of the silica particles was measured by transmission electron microscopy (TEM). The particles had diameters ranging from 245 to 455 nm with polydispersities on the order of 3.5–9.0%.

4.2.2. Synthesis of Silica-PNIPAM CS Microgels at Fixed Temperature

CS microgels were synthesized using seeded precipitation polymerizations with various feed concentrations of NIPAM as monomer and fixed ratios of the cross-linker BIS of 5 mol% (with respect to NIPAM). Eight different silica-PNIPAM CS microgel systems were synthesized following a previously published protocol using an oil bath (silicon oil) heated to 80 °C. [24] Additional CS microgels were synthesized with modified protocols described in the following: The corresponding amounts of NIPAM and BIS were dissolved in water in three-neck round-bottom flasks equipped with a reflux condenser and an overhead stirrer (KPG). The mixtures were heated in an oil bath to oil temperatures of 60–80 °C and purged with argon for one hour while stirring at the speed of 250–300 rpm. Then the respective volumes of silica core stock dispersions were added and the mixtures were further purged with nitrogen to remove oxygen. After the target temperature was reached and stabilized, the polymerizations were initiated by the rapid addition of aqueous 0.01 wt% KPS solution. The polymerizations were allowed to proceed for at least three hours. The final dispersions were hot-filtered through glass wool in a funnel and purified by repeated centrifugation for 2–8 min at 5000–7000 rcf and re-dispersion in water until the supernatant cleared. The purified dispersions were either freeze-dried for 3D assembly experiments or solvent-exchanged against ethanol via repeated centrifugation and re-dispersion in ethanol for 2D assembly experiments. Further syntheses with variation in SDS and KPS concentrations were performed on smaller scales (approx. 6 mL in total volume). All samples that were synthesized and a detailed list of all synthesis conditions and amount of materials are provided in the SI, Table S2.

4.2.3. Synthesis of Silica-PNIPAM CS Microgels Using a Temperature Ramp

A well-established temperature-ramp, surfactant-free precipitation polymerization synthesis protocol [17] was modified for the seeded polymerization with silica cores as seeds. The same setup was used as for the synthesis with the fixed temperatures described above. The reaction mixtures were equilibrated at 45 °C and purged with argon for one hour while stirring at the speed of 300 rpm. After the initiation, as soon as the appearance of turbidity was visually detected, the temperature was increased to 65 °C at the average rate of 12.6 °C/h. The polymerization was allowed to proceed for three more hours after the final temperature was reached. The microgels were purified as for the protocols at fixed temperatures.

4.3. Methods

4.3.1. Monolayer Preparation

Prior to the monolayer preparation, the glass substrates (Premium microscope slides 12-544-4, Fisher Scientific) were cut in six smaller pieces (width = 13 mm, length = 25 mm), rinsed with water and placed in a customized glass holder in a beaker for RCA-1 cleaning. The glass slides were treated in H₂O/NH₄OH/H₂O₂ solution with a volume ratio of 5:1:1 at 80 ± 5 °C for 20 min [29,30]. The monolayer was created by injecting microgel dispersions (in ethanol) directly to the air/water interface in a crystallizing dish filled with water. Three different surface pressures (approximately 10, 20 and 30 mN/m) were targeted to vary the interparticle distance of the transferred monolayer by injecting certain volumes of microgel dispersion. The monolayer was then transferred on to the glass substrate by pushing the glass substrate through the monolayer at the edge of the crystallizing dish and lifting up at the center at a steep angle (70–90°) and dried. Further details can be found in the SI.

4.3.2. Preparation of 3D Assemblies

Rectangular hollow glass tubes (5012, path length = 0.1 mm, width = 2 mm, VitroCom, Mountain Lakes, NJ, USA) were used to prepare 3D colloidal microstructures in various regimes. The concentrated dispersions were prepared from freeze-dried CS microgels re-dispersed in NMP by repeated overnight shaking (7-0045, neoLab, Heidelberg, Germany) and ultrasonication. The resulting viscous dispersion was sucked into the glass tube by an aspirator. A combination of a 10–200 µm micropipette tip and a piece of thin parafilm was used as a flexible connector between the glass tube and the aspirator. When the dispersion occupied about two thirds of the tube, the open end was sealed by using an oxyhydrogen torch. The tube containing the dispersion was then flipped upside down, cleaned and centrifuged gently. After all dispersions migrated to the sealed bottom, the other end was also sealed by the torch. The prepared samples were vertically stored until no further sedimentation was observed. The dilute samples sedimented and formed strongly iridescent colloidal crystals, whereas concentrated samples did not show any visible changes.

4.3.3. Dynamic Light Scattering (DLS)

The hydrodynamic diameter, D_h , of the CS microgels were determined using a Zetasizer Nano S (Malvern Panalytical, Kassel, Germany). The device is equipped with a HeNe laser (4 mW, 633 nm) along with a temperature-controlled jacket. Measurements were performed at a scattering angle of 173° in the temperature range between 10 and 60 °C in steps of 2 °C. Three measurements (per temperature and sample) were performed using samples filled in semi-micro PMMA cuvettes (634-0678, VWR) with 10 min of equilibration duration at each temperature. Values of D_h reported are z-average values as obtained from the measurement software. All samples had polydispersities (PDI, polydispersity index) on the order of 5–10% on average for small microgels and 10–30% for micron-sized microgels with standard deviations up to 7%.

4.3.4. Small-Angle Light Scattering (SALS)

Diffraction patterns were recorded by a self-built setup. A blue laser (LDM-20-405, 20 mW, 405 nm, MediaLas, Balingen, Germany) was used as a light source and the images were captured in the dark with a CCD camera (DCU223C-MVL6WA, Thorlabs, Bergkirchen, Germany) and a paper screen as a detector. Acquired images were grey scaled and inverted with ImageJ (1.53 k, National Institutes of Health, Bethesda, MD, USA) for better visibility. Further details can be found in the SI.

4.3.5. Transmission Electron Microscopy (TEM)

TEM measurements were performed using a JEOL JEM-2100 Plus (JEOL GmbH, Freising, Germany) microscope operated in bright-field mode at 80 kV acceleration voltage. Samples of the silica cores were prepared by applying a drop of an ethanolic particle dispersion on a carbon-coated copper grid (200 mesh, Science Services, Munich, Germany) and drying at room temperature. Samples of the CS microgels were prepared by transferring the monolayer from the air/water interface onto the copper grids, as described for the monolayer preparation. All images were subsequently processed using ImageJ.

4.3.6. Optical Light Microscopy

A Nikon Eclipse LV150N equipped with a 100× objective was used to acquire images of the microgel monolayers on the glass substrates. At least two images at different positions were recorded per sample. ImageJ was used to perform fast Fourier transformations (FFT) on the acquired images as well as to find the radial distribution function from the detected particle centers (macro version: 22 August 2011 by Ajay Gopal).

4.3.7. Confocal Laser Scanning Microscopy (CLSM)

3D samples in the glass tubes were imaged using a Zeiss LSM880 Airyscan microscope system (Zeiss Microscopy GmbH, Jena, Germany), equipped with a Plan-Apochromat 63×/1.4 oil immersion objective lens. The sample tubes were mounted on the stage on a glass slide-supported 3D-printed adapter fitting in the object holder of the motorized stage. The silica cores were covalently labeled with Rhodamine B so the samples were imaged using a 561 nm excitation laser and a BP 570–620 + LP 645 emission filter. The acquisition was performed in airyscan super-resolution mode at 1.43 (3D) or 1.52 (2D) μsec pixel dwell time and 4× line averaging. Airyscan alignment of the system was regularly checked during the acquisition process and raw stacks of the full ~100 μm range were finally processed by the Zeiss Airyscan processing in 3D standard mode. Additionally, single slice measurements were acquired at the indicated Z-depth in the middle of the glass tubes and processed in 2D standard airyscan mode.

Supplementary Materials: The following supporting information can be downloaded at: <https://www.mdpi.com/article/10.3390/gels8080516/s1>, Additional synthetic details, methods and instrumentations, more detailed description of monolayer preparation, schematics and other details on SALS setup, TEM images with a higher resolution, a brief discussion on the effect of SDS, KPS, temperature and stirring on CS microgels, fitting area fraction for monolayers (PDF), two videos of acquired z-stacks on 3D samples (AVI), and a 3D model of the multi-reactor holder for small scale synthesis (STL). Figure S1: Higher magnification TEM images of CS microgels with variously sized cores; Figure S2: Swelling curves of CS microgels synthesized with increasing SDS and KPS concentrations [31–33]; Figure S3: Swelling curves of CS microgels synthesized at various temperatures along with the comparison between two stirring methods [17,34]; Figure S4: Schematics of monolayer transfer procedure; Figure S5: The linear fit for the calculation of A_f from measured data; Figure S6: Small scale synthesis setup; Figure S7: Schematic depiction of the SALS setup used to record diffraction patterns from monolayer samples; Table S1: Chemicals used for the synthesis of silica cores presented in this paper [24]; Table S2: Chemicals and synthesis parameters used for the preparation of CS microgels presented in this work; Video S1: full z-stack of 3D sample sedimented from a dilute concentration; Video S2: full z-stack of 3D sample higher concentration with no visible sedimentation.

Author Contributions: The work consists of parts of the planned Ph.D. theses of K.K. and V.A., which are supervised by M.K. and the M.Sc. thesis of L.G., which was supervised by K.K. The conceptualization was outlined and accompanied by M.K. Synthetic studies were performed by K.K., and L.G. TEM images were recorded by C.C. Confocal microscopy was performed by S.H. under the guidance of K.K. The SALS setup was built by V.A. and modified by K.K. SALS measurements were performed by K.K. Writing of the original draft was done by K.K. and review and editing by all coauthors. Project administration and funding acquisition was done by M.K. All authors have read and agreed to the published version of the manuscript.

Funding: The authors acknowledge the DFG and the state of NRW for funding the cryo-TEM (INST 208/749-1 FUGG). M.K. acknowledges the German Research Foundation (DFG) for funding under grant KA3880/6-1. We also would like to acknowledge the Center for Advanced Imaging (CAI) at Heinrich-Heine-Universität Düsseldorf (HHU Düsseldorf) for providing access to the Zeiss LSM880 Airyscan system (Ref. No. DFG-INST 208/746-1 FUGG).

Institutional Review Board Statement: Not applicable.

Informed Consent Statement: Not applicable.

Data Availability Statement: All data of this work are included in the manuscript and the Supplementary Materials.

Acknowledgments: The authors would like to thank Marco Hildebrandt (HHU Düsseldorf) for the transferred know-how for hollow glass tube handling, Marius Otten (HHU Düsseldorf) for the additional TEM imaging, and Virginia Carrasco Fadanelli (HHU Düsseldorf) for the kind introduction to MATLAB.

Conflicts of Interest: The authors declare no conflict of interest.

References

1. Karg, M.; Pich, A.; Hellweg, T.; Hoare, T.; Lyon, L.A.; Crassous, J.J.; Suzuki, D.; Gumerov, R.A.; Schneider, S.; Potemkin, I.I.; et al. Nanogels and Microgels: From Model Colloids to Applications, Recent Developments, and Future Trends. *Langmuir* **2019**, *35*, 6231–6255. [[CrossRef](#)] [[PubMed](#)]
2. Plamper, F.A.; Richtering, W. Functional Microgels and Microgel Systems. *Acc. Chem. Res.* **2017**, *50*, 131–140. [[CrossRef](#)] [[PubMed](#)]
3. Dubbert, J.; Nothdurft, K.; Karg, M.; Richtering, W. Core-Shell-Shell and Hollow Double-Shell Microgels with Advanced Temperature Responsiveness. *Macromol. Rapid Commun.* **2015**, *36*, 159–164. [[CrossRef](#)] [[PubMed](#)]
4. Karg, M.; Pastoriza-Santos, I.; Rodríguez-González, B.; Von Klitzing, R.; Wellert, S.; Hellweg, T. Temperature, pH, and Ionic Strength Induced Changes of the Swelling Behavior of PNIPAM–Poly(allylacetic acid) Copolymer Microgels. *Langmuir* **2008**, *24*, 6300–6306. [[CrossRef](#)] [[PubMed](#)]
5. Acciaro, R.; Gilányi, T.; Varga, I. Preparation of Monodisperse Poly(N-isopropylacrylamide) Microgel Particles with Homogenous Cross-Link Density Distribution. *Langmuir* **2011**, *27*, 7917–7925. [[CrossRef](#)]
6. Schmidt, S.; Liu, T.; Rütten, S.; Phan, K.-H.; Möller, M.; Richtering, W. Influence of Microgel Architecture and Oil Polarity on Stabilization of Emulsions by Stimuli-Sensitive Core-Shell Poly(N-isopropylacrylamide-co-methacrylic acid) Microgels: Mlickering versus Pickering Behavior? *Langmuir* **2011**, *27*, 9801–9806. [[CrossRef](#)]
7. Scotti, A.; Schulte, M.F.; Lopez, C.G.; Crassous, J.J.; Bochenek, S.; Richtering, W. How Softness Matters in Soft Nanogels and Nanogel Assemblies. *Chem. Rev.* **2022**. [[CrossRef](#)]
8. Karg, M. Functional Materials Design through Hydrogel Encapsulation of Inorganic Nanoparticles: Recent Developments and Challenges. *Macromol. Chem. Phys.* **2016**, *217*, 242–255. [[CrossRef](#)]
9. Karg, M. Multifunctional inorganic/organic hybrid microgels. *Colloid Polym. Sci.* **2012**, *290*, 673–688. [[CrossRef](#)]
10. Karg, M.; Hellweg, T.; Mulvaney, P. Self-Assembly of Tunable Nanocrystal Superlattices Using Poly-(NIPAM) Spacers. *Adv. Funct. Mater.* **2011**, *21*, 4668–4676. [[CrossRef](#)]
11. Somerville, W.R.C.; Law, A.D.; Rey, M.; Vogel, N.; Archer, A.J.; Buzza, D.M.A. Pattern formation in two-dimensional hard-core/soft-shell systems with variable soft shell profiles. *Soft Matter* **2020**, *16*, 3564–3573. [[CrossRef](#)] [[PubMed](#)]
12. Menath, J.; Eatson, J.; Brilmayer, R.; Andrieu-Brunsen, A.; Buzza, D.M.A.; Vogel, N. Defined core-shell particles as the key to complex interfacial self-assembly. *Proc. Natl. Acad. Sci. USA* **2021**, *118*, e2113394118. [[CrossRef](#)] [[PubMed](#)]
13. Humphreys, B.A.; Prescott, S.W.; Murdoch, T.J.; Nelson, A.; Gilbert, E.P.; Webber, G.B.; Wanless, E.J. Influence of molecular weight on PNIPAM brush modified colloidal silica particles. *Soft Matter* **2019**, *15*, 55–64. [[CrossRef](#)] [[PubMed](#)]
14. Asai, M.; Zhao, D.; Kumar, S.K. Role of Grafting Mechanism on the Polymer Coverage and Self-Assembly of Hairy Nanoparticles. *ACS Nano* **2017**, *11*, 7028–7035. [[CrossRef](#)] [[PubMed](#)]
15. Cors, M.; Wrede, O.; Genix, A.-C.; Anselmetti, D.; Oberdisse, J.; Hellweg, T. Core-Shell Microgel-Based Surface Coatings with Linear Thermoresponse. *Langmuir* **2017**, *33*, 6804–6811. [[CrossRef](#)] [[PubMed](#)]

16. Schmid, A.J.; Dubbert, J.; Rudov, A.A.; Pedersen, J.S.; Lindner, P.; Karg, M.; Potemkin, I.I.; Richtering, W. Multi-Shell Hollow Nanogels with Responsive Shell Permeability. *Sci. Rep.* **2016**, *6*, 22736. [[CrossRef](#)]
17. Meng, Z.; Smith, M.H.; Lyon, L.A. Temperature-programmed synthesis of micron-sized multi-responsive microgels. *Colloid Polym. Sci.* **2009**, *287*, 277–285. [[CrossRef](#)]
18. Tang, J.S.J.; Bader, R.S.; Goerlitzer, E.S.A.; Wendisch, J.F.; Bourret, G.R.; Rey, M.; Vogel, N. Surface Patterning with SiO₂@PNiPAm Core–Shell Particles. *ACS Omega* **2018**, *3*, 12089–12098. [[CrossRef](#)]
19. Vasudevan, S.A.; Rauh, A.; Barbera, L.; Karg, M.; Isa, L. Stable in Bulk and Aggregating at the Interface: Comparing Core–Shell Nanoparticles in Suspension and at Fluid Interfaces. *Langmuir* **2018**, *34*, 886–895. [[CrossRef](#)]
20. Büchel, G.; Grün, M.; Unger, K.K.; Matsumoto, A.; Kazuo, T. Tailored syntheses of nanostructured silicas: Control of particle morphology, particle size and pore size. *Supramol. Sci.* **1998**, *5*, 253–259. [[CrossRef](#)]
21. Kurka, D.W.; Niehues, M.; Kudruk, S.; Gerke, V.; Ravoo, B.J. Polythiolactone—Decorated Silica Particles: A Versatile Approach for Surface Functionalization, Catalysis and Encapsulation. *Chem. Eur. J.* **2021**, *27*, 7667–7676. [[CrossRef](#)] [[PubMed](#)]
22. Karg, M.; Wellert, S.; Prevost, S.; Schweins, R.; Dewhurst, C.; Liz-Marzán, L.M.; Hellweg, T. Well defined hybrid PNIPAM core-shell microgels: Size variation of the silica nanoparticle core. *Colloid Polym. Sci.* **2011**, *289*, 699–709. [[CrossRef](#)]
23. Vasudevan, S.A.; Rauh, A.; Kröger, M.; Karg, M.; Isa, L. Dynamics and Wetting Behavior of Core–Shell Soft Particles at a Fluid–Fluid Interface. *Langmuir* **2018**, *34*, 15370–15382. [[CrossRef](#)] [[PubMed](#)]
24. Rauh, A.; Rey, M.; Barbera, L.; Zanini, M.; Karg, M.; Isa, L. Compression of hard core–soft shell nanoparticles at liquid–liquid interfaces: Influence of the shell thickness. *Soft Matter* **2017**, *13*, 158–169. [[CrossRef](#)] [[PubMed](#)]
25. Ruseva, V.; Lyons, M.; Powell, J.; Austin, J.; Malm, A.; Corbett, J. Capillary dynamic light scattering: Continuous hydrodynamic particle size from the nano to the micro-scale. *Colloids Surf. A Physicochem. Eng. Asp.* **2018**, *558*, 504–511. [[CrossRef](#)]
26. Ruseva, V.; Jankevics, H.; Corbett, J. An optimized filling method for capillary DLS. *MethodsX* **2019**, *6*, 606–614. [[CrossRef](#)]
27. Stöber, W.; Fink, A.; Bohn, E. Controlled growth of monodisperse silica spheres in the micron size range. *J. Colloid Interface Sci.* **1968**, *26*, 62–69. [[CrossRef](#)]
28. Bogush, G.; Tracy, M.; Zukoski Iv, C. Preparation of monodisperse silica particles: Control of size and mass fraction. *J. Non-Cryst. Solids* **1988**, *104*, 95–106. [[CrossRef](#)]
29. Kern, W. Cleaning solution based on hydrogen peroxide for use in silicon semiconductor technology. *RCA Rev.* **1970**, *31*, 187–205.
30. Brasse, Y.; Müller, M.B.; Karg, M.; Kuttner, C.; König, T.A.F.; Fery, A. Magnetic and Electric Resonances in Particle-to-Film-Coupled Functional Nanostructures. *ACS Appl. Mater. Interfaces* **2018**, *10*, 3133–3141. [[CrossRef](#)]
31. Wu, X.; Pelton, R.H.; Hamielec, A.E.; Woods, D.R.; McPhee, W. The kinetics of poly(N-isopropylacrylamide) microgel latex formation. *Colloid Polym. Sci.* **1994**, *272*, 467–477. [[CrossRef](#)]
32. Andersson, M.; Maunu, S.L. Structural studies of poly(N-isopropylacrylamide) microgels: Effect of SDS surfactant concentration in the microgel synthesis. *J. Polym. Sci. Part B Polym. Phys.* **2006**, *44*, 3305–3314. [[CrossRef](#)]
33. Andersson, M.; Maunu, S.L. Volume phase transition and structure of poly(N-isopropylacrylamide) microgels studied with ¹H-NMR spectroscopy in D₂O. *Colloid Polym. Sci.* **2006**, *285*, 293–303. [[CrossRef](#)]
34. Still, T.; Chen, K.; Alsayed, A.M.; Aptowicz, K.B.; Yodh, A. Synthesis of micrometer-size poly(N-isopropylacrylamide) microgel particles with homogeneous crosslinker density and diameter control. *J. Colloid Interface Sci.* **2013**, *405*, 96–102. [[CrossRef](#)]